

Evidence of the influence of magnetism on pseudogap states in the high resolution spectra of EuFe_2As_2

Ganesh Adhikary, Nishaina Sahadev, Deep Narayan Biswas, R. Bindu,
Neeraj Kumar, A. Thamizhavel, S. K. Dhar and Kalobaran Maiti*

*Department of Condensed Matter Physics and Materials Science,
Tata Institute of Fundamental Research, Homi Bhabha Road, Colaba, Mumbai - 400 005, INDIA.*
(Dated: July 9, 2018)

Employing *state of the art* high resolution photoemission spectroscopy, we studied the temperature evolution of the electronic structure of EuFe_2As_2 , an unique pnictide, where antiferromagnetism of Eu layer survives within the superconducting phase due to ‘FeAs’ layers achieved via substitution and/or pressure. High energy and angle resolution helped to reveal pseudogap-quasiparticle features having primarily As 4*p* character and spin density wave transition induced band folding in the electronic structure. A weakly dispersing feature of dominant As 4*p* character is discovered around 80 meV that becomes weaker in intensity below 20 K manifesting influence of antiferromagnetic order on conduction electrons. These results provide an evidence of a link between the pseudogap states and magnetism that could be revealed employing high resolutions.

PACS numbers: 74.20.Mn, 71.20.-b, 74.70.-b, 75.30.Fv, 79.60.-i

Interplay of magnetism and superconductivity is a long standing issue in material research and believed to play the key role in deriving the unconventional superconductivity [1]. Discovery of superconductivity in Fe-based compounds [2, 3] via suppression of spin density wave (SDW) state, further reinforces this connection and are believed to be good candidates for such studies. These superconductors are usually classified into the following categories based on their composition and structure, namely ‘1111’, ‘122’, ‘111’ and ‘11’ families [4]. ‘FeAs’ layers play the key role in deriving the materials properties of these systems. Among them, ‘122’ class of materials, $A\text{Fe}_2\text{As}_2$ ($A = \text{Ba}, \text{Sr}, \text{Ca}$ and Eu) have drawn significant attention as high quality single crystals can be grown easily in the whole composition range and one can easily tailor the properties of the materials via insertion of varied elements in the layers intermediate to the ‘FeAs’ layers.

EuFe_2As_2 is a special compound in this class as the spacer atom, Eu has large moment leading to two magnetic transitions, (i) SDW-type antiferromagnetic transition around 190 K due to Fe-moments and (ii) antiferromagnetic (AFM) ordering of the Eu-moments at 20 K. The versatility of EuFe_2As_2 is that superconductivity (SC) can be achieved by substituting foreign elements in any of the sites. For example, substitution of K [5, 6] and Na [7] at Eu sites leads to superconductivity with transition temperature, T_C as high as 30 K and 34.7 K, respectively. Fe site substitution by Co results in superconductivity [8, 9]. Ni substitution at Fe sites is multifaceted; while Ni-doped CaFe_2As_2 is superconducting [10], Eu moments align ferromagnetically in Ni-doped EuFe_2As_2 at low temperatures and no superconductivity was observed [11]. The phase diagram of P-doping at As sites is also interesting [12, 13]; a narrow low-doped regime exhibit coexistence of superconductivity and AFM order,

while a somewhat higher doping leads to ferromagnetic order of Eu-moments and superconductivity disappears. Application of pressure leads to superconductivity even in the parent compound [14]. Evidently, EuFe_2As_2 provides an ideal playground to achieve insight on the interplay of superconductivity and magnetism. Here, we studied the evolution of the electronic structure as a function of temperature and photon energy employing high resolution photoemission spectroscopy. Experimental results provide signature of pseudogap, features related to magnetic order and evidence of a link between them.

High quality single crystalline, EuFe_2As_2 was grown using Sn-flux[15]. The photoemission measurements were carried out on cleaved sample surface using monochromatic photon sources and Gammadata Scienta, R4000 WAL analyzer at a base pressure better than 3×10^{-11} torr. The temperature variation down to 10 K on the sample was achieved using an open cycle liquid helium cryostat, LT-3M from Advanced Research Systems, USA. The energy resolution was fixed to 2 meV for angle integrated photoemission (AIPES) and 10 meV for angle-resolved photoemission spectroscopy (ARPES) with angle resolution set to 0.3° .

We probed the evolution of the electronic structure of EuFe_2As_2 as a function of temperature and photon energy employing high energy resolution in the angle integrated photoemission (AIPES) mode. The valence band using He I ($h\nu = 21.2$ eV) and He II ($h\nu = 40.8$ eV) photon energies at 10 K and 30 K are shown in Fig. 1(a). He II spectra exhibit three distinct peaks around 0.1, 1.2 and 1.7 eV binding energies. The intensities of the 1.2 and 1.7 eV features become significantly weak in the He I spectra relative to the 0.1 eV feature intensity. In addition, the peak A in He II spectra is slightly shifted (feature B) in the He I spectra. A change in photon energy from He I to He II excitations leads to a significant increase in

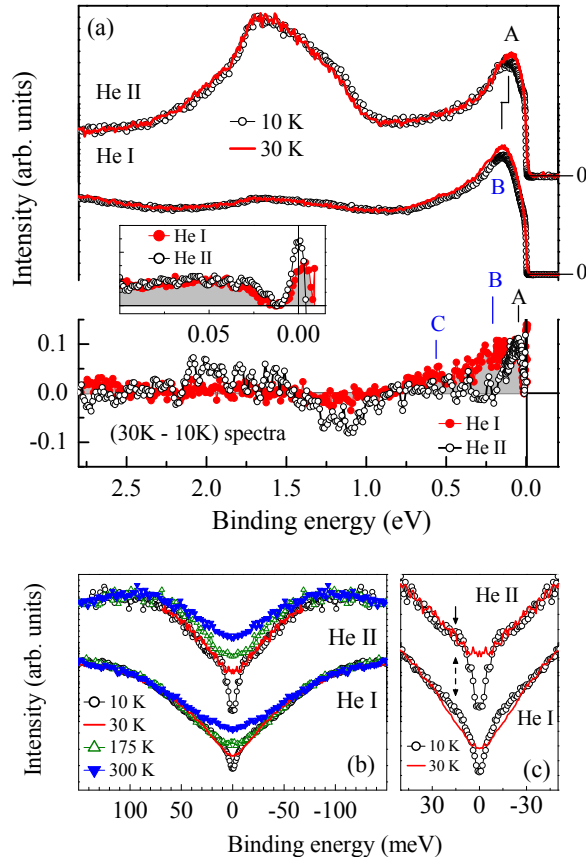


FIG. 1: (color online) (a) High resolution He I and He II spectra at 10 K (symbols) and 30 K (lines). The subtracted spectra (30 K - 10 K) at He I (solid circles) and He II (open symbols) are shown in the lower panel. The inset shows the subtracted spectra near Fermi level. (b) Symmetrized spectra at He I and He II energies as a function of temperature. (c) Symmetrized 10 K and 30 K spectra near Fermi level.

photoemission cross-section of Eu $4f$ states ($\sigma(Eu4f)$) compared to all other contributions in the valence band [16]. Thus, the features in 1-2 eV energy range can be attributed primarily to the Eu $4f$ photoemission [17] and the intensities near the Fermi level, ϵ_F are due to Fe $3d$ - As $4p$ hybridized bands. The change in lineshape and peak positions reflect the sensitivity of the spectra to the photoemission cross section of constituent electronic states.

Change in temperature across the AFM transition of the Eu moments leads to a decrease in intensity near ϵ_F - this is evident in the subtracted spectra (30 K - 10 K) shown in the lower panel of Fig. 1(a) exhibiting three distinct features, A, B and C. The feature, A appearing around 50 meV (see inset for clarity) has similar intensity in both He I and He II spectra suggesting mixed character of these states. The feature, B at about 200 meV is

strong in He I spectrum and absent in He II spectrum. At He I and He II energies, the values of $\sigma(Fe3d)$ are 4.833 and 8.751, and that of $\sigma(As4p)$ are 3.856 and 0.2949, respectively[16]. Clearly, As $4p$ is significantly stronger in He I energies, while Fe $3d$ contributions are stronger in He II energies. This indicates dominance of As $4p$ character in feature B. The feature, C appearing around 0.5 eV is weak and observed in the He I spectrum indicating its As $4p$ character. The intensity changes beyond 1 eV is visible primarily in He II spectrum presenting the changes in Eu $4f$ intensities. Clearly, the electronic states near ϵ_F possess finite As $4p$ contributions due to Eu $4f$ -As $4p$ and Fe $3d$ -As $4p$ hybridizations, and are highly sensitive to the AFM ordering. Similar intensity of the feature A indicates participation of Fe $3d$ states in the AFM ordering.

In Fig. 1(b) and 1(c), we investigate the spectral density of states (SDOS) obtained by symmetrization ($I(\epsilon - \epsilon_F) + I(\epsilon_F - \epsilon)$) of the experimental data, which provides a good estimation of the intensity at ϵ_F . The SDOS at both the photon energies (He I and He II) exhibit significant reduction of intensity at ϵ_F across SDW transition. The high energy resolution enabled to reveal an additional gap at ϵ_F across the AFM transition at 20 K and a quasiparticle peak appears around 20 meV in both He I and He II spectra as evidenced in the rescaled spectra in Fig. 1(c). While AFM transition can lead to a gap/depletion at ϵ_F [18, 19], the spectral evolution exhibiting a pseudogap-quasiparticle peak structure in Fig. 1(c) resembles the widely known spectral evolution in various unconventional superconductors exhibiting precursor effects [20, 21] noting the fact that EuFe_2As_2 is highly susceptible to show superconductivity as it exhibits superconductivity under application of pressure and/or suitable substitution at any of the three sites.

Various angle resolved photoemission (ARPES) studies of EuFe_2As_2 showed that the temperature change across the SDW transition (~ 190 K) leads to the formation of tiny hole and electron pockets near (π, π) [22]. The overlap of the back-folded and non-folded bands in the SDW phase forms small ‘droplets’ in the Fermi surface [23]. Both, the bulk measurements [17] and ARPES studies [22] suggested that Eu and FeAs sublattices are nearly decoupled as no noticeable change was observed across the antiferromagnetic ordering. However, the high energy resolution employed in this study helped to reveal strong evidence of the influence of antiferromagnetic transition on the conduction electrons responsible for the electronic properties. In order to probe this in more detail, we study the energy bands around the Γ point along $(0,0)$ - (π, π) direction as a function of temperature and photon energy.

In Fig. 2(a), 2(b) and 2(c), we show the He II ARPES data at 300 K, 30 K and 10 K, respectively - the lower panels show their second derivative. The band dispersions at 300 K (paramagnetic phase) are consistent

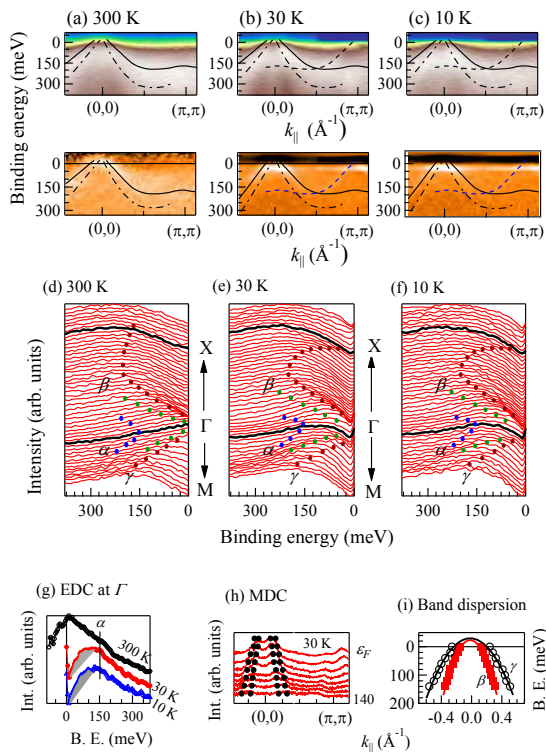


FIG. 2: (color online) He II ARPES data along $(0,0)$ - (π,π) -direction at (a) 300 K, (b) 30 K and (c) 10 K. The lower panel show the second derivative of the same data. Lines are guide to the eye. The corresponding EDCs at (d) 300 K, (e) 30 K and (f) 10 K. (g) EDC at Γ at different temperatures. (h) MDC at 30 K. The points in (h) and (i) represent the peak positions obtained by fitting MDCs shown in (h).

with the band structure results [22]. At 30 K, the region around (π,π) modifies significantly - the dispersion around (π,π) becomes very similar to that at Γ point indicating band folding due to the supercell formation in the SDW phase evidencing signature of a hole pocket around (π,π) . We calculated SDOS by dividing the experimental spectra by the resolution broadened Fermi-Dirac distribution function. The corresponding energy distribution curves (EDCs) are shown in Fig. 2(d), 2(e) and 2(f) for the spectra at 300 K, 30 K and 10 K, respectively. Three distinct bands denoted by α , β and γ are discernible in the spectra. While the α band folds back around 150 meV binding energy at Γ point, β and γ bands cross ϵ_F forming hole pockets around Γ point [22, 23].

The energy band dispersions of β and γ bands were derived via fitting the momentum distribution curves (MDC). The peak positions are shown in Fig. 2(h) and 2(i). The estimated values of k_F for the β and γ bands are about 0.1 \AA^{-1} and 0.2 \AA^{-1} , respectively. The effective mass ($m^*/m_e = \hbar^2/(\partial^2\epsilon/\partial k^2)$) of the charge carriers

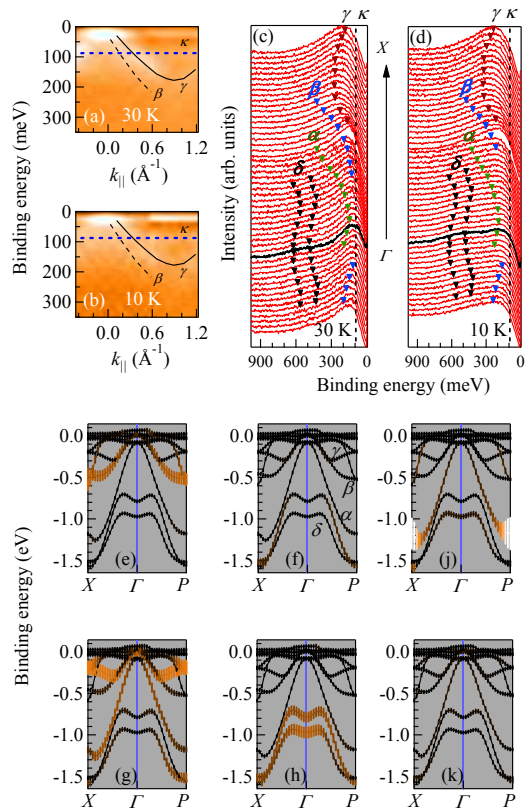


FIG. 3: (color online). Second derivative of the He I ARPES data along ΓM -direction at (a) 30 K and (b) 10 K. EDCs of the SDOS of corresponding spectra at (c) 30 K and (d) 10 K. Calculated energy bands near Fermi level highlighting the (e) Fe $3d_{xy}$, (f) Fe $3d_{x^2-y^2}$, (g) Fe $3d_{xz}+3d_{yz}$, (h) Fe $3d_{z^2}$, (j) As $4p_z$ and (k) As $4p_x+4p_y$. The intensity of the As $4p$ states are magnified by 10 times.

is found to be 2.5 and 6.1 for the β and γ bands, respectively, consistent with the values estimated from quantum oscillation studies in similar systems [24]. The electronic states forming the γ band are found to be more correlated than others and play active role in the SDW transition. The Fermi velocities for the two bands are 6.5×10^4 and 4.5×10^4 m/sec, respectively. These values remain almost the same across the antiferromagnetic transition at 20 K.

The EDC around Γ point exhibit interesting evolution with temperature. At 300 K, EDC exhibits large intensity near ϵ_F . The 30 K data, on the other hand, exhibits a dip at ϵ_F , which becomes more prominent at 10 K consistent with the AIPES data. This is shown with better clarity in Fig. 2(g), where we show the EDCs at Γ point at various temperatures. The α band appearing around 150 meV remains almost unchanged in the whole temperature range studied. An additional feature (see the

shaded area) appears around 80 meV in the 30 K spectrum that reduced significantly in the 10 K data. To get a better understanding of this feature, we investigated the He I spectra along the same k -direction at 30 K and 10 K in Fig. 3. The β and γ bands remain two dimensional in the whole temperature range and hence, the difference in the values of k_z probed by He I ($\sim 10\pi/c$) and He II ($\sim 13\pi/c$), will have negligible influence on the dispersions [25]. The dispersion of the β and γ bands are evident in Fig. 3(a) and 3(b), and in the EDCs of the SDOS shown in Fig. 3(c) and 3(d) as well. In addition, a weakly dispersing feature around 80 meV denoted by κ is observed.

We have calculated the energy bands and their orbital characters using *state-of-the-art* full potential linearized augmented plane wave method within the local density approximations using Wien2k software [26]. The calculated energy bands corresponding to the experimental data are shown in the figure, where the thickness of the lines represent the orbital character to be 3(e) Fe $3d_{xy}$, 3(f) Fe $3d_{x^2-y^2}$, 3(g) Fe $3d_{xz}+3d_{yz}$, 3(h) Fe $3d_{z^2}$, 3(j) As $4p_z$ and (k) As $4p_x+4p_y$ derived. The calculated results, consistent with the results in literature for various similar systems, resemble well the experimental data. The δ bands possessing d_{z^2} character appear at higher binding energies. The α and β bands possess (d_{xz}, d_{yz}) and d_{xy} character, respectively and are less influenced by the magnetic transitions - a small shift (~ 20 meV) of the β band is observed across the AFM transition at 20 K. Fig. 3(g) indicates (d_{xz}, d_{yz}) symmetry of the γ band, which is responsible for the SDW transition. This is understandable as the As layers appear above and below the Fe-layers and hence, the hybridization mediating inter-cite coupling will be dominated by (d_{xz}, d_{yz}) electronic states.

Although the energy bands in the vicinity of ϵ_F possess dominant Fe $3d$ character, the contribution of As $4p$ states is significant due to hybridization among the corresponding electronic states. In order to investigate the feature, κ further, we compare the EDCs at 30 K and 10 K observed in He I and He II spectra in Fig. 4. While the photoemission intensities reduce with temperature in both the photon energies, the largest change is observed in the He I spectra. The relative photoemission cross section of the As $4p$ states is enhanced significantly at He I energy compared to that at He II energy [16]. Thus, the feature κ can be attributed primarily to As $4p$ states. Weak dispersion suggests hybridization of these states with the weakly dispersing Eu $4f$ states. This characterization is further justified by the fact that the intensity of the κ band reduces significantly with the decrease in temperature across the AFM transition temperature due to Eu $4f$ moments. The symmetrized Spectral DOS are shown in Figs. 4(c) and 4(d) for He I and He II excitations, respectively. The largest change in SDOS is observed at k -points, where the β and γ bands cross the

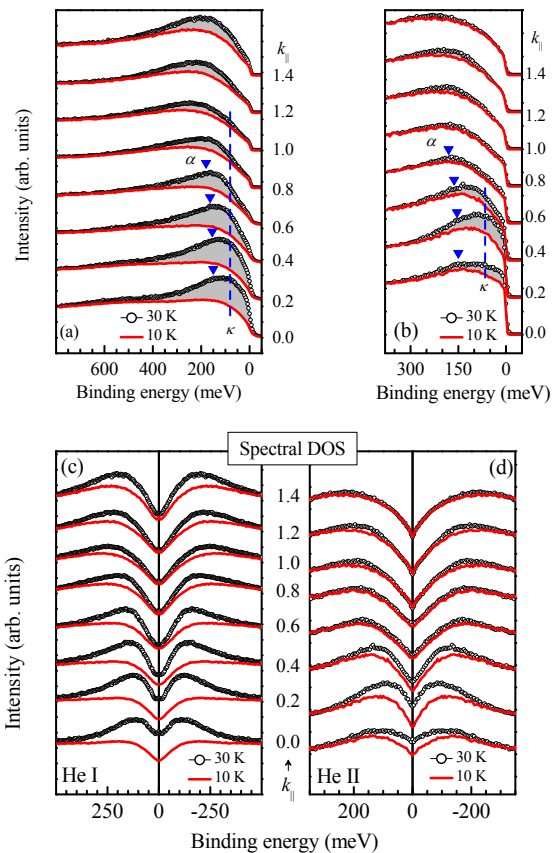


FIG. 4: (color online). EDCs at different k -points in the (a) He I and (b) He II spectra. The shaded area show the change across antiferromagnetic transition. The SDOS at 10 K (lines) and 30 K (open circles) obtained by symmetrization of the raw data at different k -points at (c) He I and (d) He II photon energies.

Fermi level - the intensities at all other k -points are almost identical. The change in intensity is largest in the He I spectra indicating again large As $4p$ character of these electronic states.

In summary, we studied the temperature evolution of the electronic structure of EuFe_2As_2 , an ideal compound to study the interplay between magnetism and superconductivity generally known to be two mutually exclusive phenomena. The signature of pseudogap-quasiparticle feature, typical of various superconducting materials is manifested in the high resolution data at low temperatures; these features possess large As $4p$ character. The angle resolved data demonstrate band folding due to the spin density wave transition. Distinct signature of an additional weakly dispersing feature is manifested in the low temperature data possessing large As $4p$ character that reduces in intensity across antiferromagnetic tran-

sition in the Eu layer. Evidently, the Eu $4f$ -As $4p$ and Fe $3d$ -As $4p$ hybridizations are significant and play major role in deriving the electronic properties. These results demonstrate evidence of a link of antiferromagnetism and pseudogap states that could be revealed due to the employment of high resolutions.

The authors KM and NS acknowledge the financial support from the Department of Science and Technology, Government of India under the ‘Swarnajayanti Fellowship programme’.

* Corresponding author: kbmaiti@tifr.res.in

- [1] K. Jin, N. P. Butch, K. Kirshenbaum, J. Paglione, and R. L. Greene, *Nature* **476**, 73 (2011).
- [2] Y. Kamihara, H. Hiramatsu, M. Hirano, R. Kawamura, H. Yanagi, T. Kamiya, and H. Hosono, *J. Am. Chem. Soc.* **128**, 10012 (2006).
- [3] Y. Kamihara, T. Watanabe, M. Hirano, and H. Hosono, *J. Am. Chem. Soc.* **130**, 3296 (2008).
- [4] K. Ishida, Y. Nakai, H. Hosono, *J. Phys. Soc. Jpn.* **78**, 062001 (2009).
- [5] H. S. Jeevan, Z. Hossain, D. Kasinathan, H. Rosner, C. Geibel, and P. Gegenwart, *Phys. Rev. B* **78**, 092406 (2008).
- [6] Anupam, P. L. Paulose, H. S. Jeevan, C. Geibel, and Z. Hossain, *J. Phys.: Condens. Matter* **21**, 265701 (2009).
- [7] Y. Qi, Z. Gao, L. Wang, D. Wang, X. Zhang and Y. Ma, *New J. Phys.* **10** 123003 (2008).
- [8] C. XiaoBo, R. ZhiAn, D. HongSheng, and L. LiHua, *SCIENCE CHINA* **53** 1212 (2010).
- [9] M. Matusiak, Z. Bukowski, and J. Karpinski *Phys. Rev. B* **83**, 224505 (2011).
- [10] N. Kumar, S. Chi, Y. Chen, Kumari G. Rana, A. K. Nigam, A. Thamizhavel, W. Ratcliff, S. K. Dhar, and J. W. Lynn, *Phys. Rev. B* **80**, 144524 (2009).
- [11] Z. Ren, X. Lin, Q. Tao, S. Jiang, Z. Zhu, C. Wang, G. Cao, and Z. Xu, *Phys. Rev. B* **79**, 094426 (2009).
- [12] I. Nowik1, I. Felner, Z. Ren, G. H. Cao, and Z. A. Xu, *J. Phys.: Condens. Matter* **23** 065701 (2011).
- [13] H. S. Jeevan, D. Kasinathan, H. Rosner, and P. Gegenwart, *Phys. Rev. B* **83**, 054511 (2011).
- [14] N. Kurita, M. Kimata, K. Kodama, A. Harada, M. Tomita, H. S. Suzuki, T. Matsumoto, K. Murata, S. Uji, and T. Terashima, *Phys. Rev. B* **83**, 214513 (2011).
- [15] Y. Xiao, Y. Su, M. Meven, R. Mittal, C. M. N. Kumar, T. Chatterji, S. Price, J. Persson, N. Kumar, S. K. Dhar, A. Thamizhavel, and Th. Brueckel, *Phys. Rev. B* **80**, 174424 (2009).
- [16] J. J. Yeh and I. Lindau, *At. Data and Nucl. Data Tables* **32**, 1 (1985).
- [17] H. S. Jeevan, Z. Hossain, D. Kasinathan, H. Rosner, C. Geibel, *P. Gegenwart Phys. Rev. B* **78**, 052502 (2008).
- [18] R. S. Singh, V. R. R. Medicherla, and K. Maiti, *Appl. Phys. Lett.* **91**, 132503 (2007); G. Adhikary, R. Bindu, S. Patil and K. Maiti, *Appl. Phys. Lett.* **100**, 042401 (2012).
- [19] R. Bindu, G. Adhikary, S. K. Pandey, S. Patil and K. Maiti, *New J. Phys.* **12** 033003 (2010); R. Bindu, G. Adhikary, N. Sahadev, N. P. Lalla, and K. Maiti, *Phys. Rev. B* **84**, 052407 (2011).
- [20] A. Kanigel, M. R. Norman, M. Randeria, U. Chatterjee, S. Souma, A. Kaminski, H. M. Fretwell, S. Rosenkranz, M. Shi, T. Sato, T. Takahashi, Z. Z. Li, H. Raffy, K. Kadowaki, D. Hinks, L. Ozyuzer, and J. C. Campuzano, *Nat. Phys.* **2**, 447 (2006).
- [21] V. R. R. Medicherla, S. Patil, R. S. Singh, and K. Maiti, *Appl. Phys. Lett.* **90**, 062507 (2007).
- [22] B. Zhou *et al.*, *Phys. Rev. B* **81**, 155124 (2010).
- [23] S. de Jong *et al.*, *Europhys. Letts.* **89**, 27007 (2010).
- [24] S. E. Sebastian, J. Gillett, N. Harrison, P. H. C. Lau, C. H. Mielke, and G. G. Lonzarich, *J. Phys.: Condens. Matter* **20**, 422203 (2008); J. G. Analytis, R. D. McDonald, J.-H. Chu, S. C. Riggs, A. F. Bangura, C. Kucharczyk, M. Johannes, and I. R. Fisher, *Phys. Rev. B* **80**, 064507 (2009).
- [25] C. Liu, T. Kondo, N. Ni, A. D. Palczewski, A. Bostwick, G. D. Samolyuk, R. Khasanov, M. Shi, E. Rotenberg, S. L. Budko, P. C. Canfield, and A. Kaminski, *Phys. Rev. Lett.* **102**, 167004 (2009); S. Thirupathiah, E. D. L. Rienks, H. S. Jeevan, R. Ovsyannikov, E. Slooten, J. Kaas, E. van Heumen, S. de Jong, H. A. Dürr, K. Siemensmeyer, R. Follath, P. Gegenwart, M. S. Golden, and J. Fink, *Phys. Rev. B* **84**, 014531 (2011).
- [26] P. Blaha, K. Schwarz, G. K. H. Madsen, D. Kvasnicka, and J. Luitz, **WIEN2k**, An Augmented Plane Wave + Local Orbitals Program for Calculating Crystal Properties (Karlheinz Schwarz, Techn. Universität Wien, Austria), 2001. ISBN 3-9501031-1-2.